Quantum wires in staggered-band-line-up single heterostructures with corrugated interfaces

V. Türck, O. Stier, F. Heinrichsdorff, M. Grundmann, and D. Bimberg
Institut für Festkörperphysik, TU Berlin, Hardenbergstraße 36, D-10623 Berlin, Germany

(Received 20 August 1996)

The spatial shape of the conduction- and valence-band edges of type-II heterojunctions in V grooves is calculated self-consistently. Quantum wires are formed in the groove center only by means of a deformed potential shape without any further structural confinement. The quantum-wire potential is attractive for one type of charge carrier only and repulsive for the other type. The influence of structural parameters on the formation of the wire and on the quantum states is studied. As a model system we use InP on $In_{0.48}Al_{0.52}As$ in which an electron wire is formed. Structures with periodic arrays of grooves that exhibit a significantly deeper lateral potential than single grooves are investigated. In those structures an influence of the adjacent side quantum well can no longer be observed. We find here a subband splitting somewhat smaller than kT at room temperature and strongly depending on the ''sharpness'' of the groove tip. A comparison of self-consistent calculations and the often used semiclassical calculations shows that the latter method is liable to produce incorrect quantitative results. [S0163-1829(97)03211-6]

I. INTRODUCTION

The study of low-dimensional semiconductor structures has recently become the focus of interest in semiconductor physics. Much effort has gone into the fabrication of low-dimensional structures like quantum wells,[1,2] quantum wires,[3–5] and quantum dots.[6–8] Fabrication methods make use of self-organization processes in order to obtain one-dimensional and zero-dimensional structures, thus making redundant post-growth structuring and etching processes. Theoretical studies predict interesting features of these low-dimensional structures and their possible usefulness for the design, e.g., of lasers with interesting properties.[9] Though most of this work was done with nested type-I heterostructures, there has nevertheless been significant progress in the study of staggered type-II heterostructures.[10] The formation of spatially separated confinement potentials for electrons and holes on either side of an interface has been observed directly for quantum wells[11,12] and quantum dots,[13–15] and has been modeled theoretically.[16] Applications for devices like long-wavelength detectors[17] and tunable-light emitters[18,19] have been presented, and even the observation of laser emission has been reported.[20]

Along with the improvement of fabrication methods, theoretical modeling has become essential because numerical simulations can stimulate the development of structures and reduce the number of experiments necessary to design the optimal structure of a device. In the field of quantum wires the research on their band structure focuses on two main areas. One is the calculation of the complex band structure in simplified geometries[21–23] in order to obtain precise predictions of energy dispersion, masses, and densities of states, and the other is the detailed calculation of spatial contours of the band edges[24,25] in order to estimate recombination energies and probabilities.

The spatial dependence of the band edges in quantum wires has been calculated for different shapes and geometries. However, in most cases only semiclassical calculations were performed. The first fully self-consistent calculations were presented by Laux and Stern for narrow gate-induced wires in silicon.[26] Later Kerkhoven *et al.* presented self-consistent calculations for field induced quantum wires[27] as well, and for quantum wires in corrugated type-I double heterostructures.[28] Wu and Ruden presented self-consistent results for quantum wires under etched ridges.[29] In addition to these calculations, which were performed for rather realistic systems, several structures of simplified geometry have been calculated self-consistently, like wires with cylindrical[30,31] or rectangular cross sections.[32] Such structures are more of general and theoretical interest.

The formation of an electron quantum wire in a heterojunction on a corrugated substrate was predicted by Sawada *et al.*, who proposed a modulation-doped $GaAs/Al_xGa_{1-x}As$ junction in a V groove,[33] and presented results of semiclassical calculations later.[34] Porod, Harbury, and Goodnick proposed a $GaAs/Al_xGa_{1-x}As$ junction in a groove with an additional lateral pn doping introduced by selective Si doping, and later presented results of a semiclassical calculation.[35]

Up to now, to our knowledge, no self-consistent calculations for quantum wires formed on single heterojunctions in V grooves have been presented. However, self-consistent calculations are essential to obtain realistic results for those structures, because the energy of confined states is close to the Fermi energy, and thus the thermal population of the subbands is high. All semiclassical calculations for such structures have been based on idealized geometries, the possible influence of deviations has not been considered. Finally, the concept of quantum wires on single heterojunctions in V grooves has not been extended to type-II interfaces although here interesting effects are to be expected.

This paper deals with the self-consistent calculation of quantum wires formed in corrugated type-II single heterojunctions. Section II describes the theoretical basics of the calculation, and Sec. III the numerical methods used for the calculation. The results are presented and discussed in Sec. IV, and Sec. V contains the conclusions we arrived at.

 © 1997 The American Physical Society

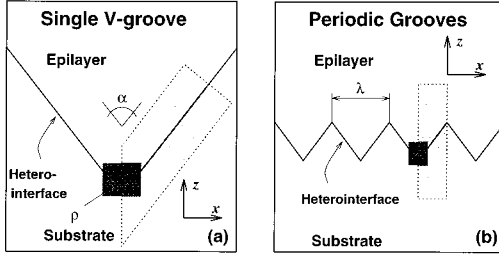

FIG. 1. Model of the buried V-groove heterojunction for (a) a single groove and (b) a periodic ensemble of grooves. The structure is determined by the parameters α (the angle enclosed by the sidewalls) and ρ (the radius of curvature of the groove bottom). Besides α and ρ, the periodic structure is described by the parameter λ (the lateral groove period). The light gray shaded areas are the domains of solution for the Poisson equation, and the dark gray ones are the respective Schrödinger boxes. Note that the domains are not given true to scale, but that the Schrödinger box is oversized.

II. APPROACH

In this paper we investigate deeply buried single V-groove heterojunctions [see Fig. 1(a)] and periodically grooved structures in which the grooves are separated by triangular ridges with a groove period λ smaller than 0.5 μm [see Fig. 1(b)].

This kind of grooved structures can be fabricated, e.g., by overgrowing V shaped grooves etched into a substrate. This method has been used in the production of GaAs-based[3] or InP-based[36,37] double heterostructure type-I quantum wires.

An ideal V groove is mathematically described by the angle α formed by its sidewalls. We introduce a second parameter in order to describe the realistic deviation from the ideally sharp V shape:[3] the groove tip is approximated by a circular segment of radius ρ. This allows us to take into account rounding effects which occur during etching or growth.

For our model calculations we assume a quantum wire of infinite length extended along the y axis. In order to describe this system, the shapes of the valence and conduction band edges in the (x-z) plane must be calculated. The spatial shape of the conduction-band edge $E_C(x,z)$ is determined by the electrostatic potential $e\Phi$ as

$$E_C(x,z)=E_0-e\Phi(x,z)-\chi(x,z),$$

where $\chi(x,z)$ describes the electron affinity and E_0 is the vacuum level. χ is a material parameter, and the difference of the electron affinities of two materials equals the conduction-band offset. The electrostatic potential $e\Phi$ is the solution of the two-dimensional Poisson equation

$$\mathrm{div}[\epsilon(x,z)\mathrm{grad}\Phi(x,z)]=-\rho(x,z). \tag{1}$$

$\epsilon(x,z)$ is the dielectric constant, and $\rho(x,z)$ is the classical charge density obtained from Fermi-Dirac statistics. To simplify matters the Fermi integral $F_{1/2}(z)$ is often replaced by the Boltzmann approximation. This is only admissible, however, if the energetic difference between the Fermi energy and the band edges is significantly larger than kT. We do not use the Boltzmann approximation here since we want to calculate device structures at room temperature.

The *classical* description is not appropriate for a charged quantum structure because quantum effects are not taken into account. The *semiclassical* method uses a classically calculated potential on which the Schrödinger equation is solved *once* to compute quantum levels. If the population of the corresponding subbands is very small, which is always the case if their energetic distance to the Fermi energy is significantly larger than kT, the semiclassical method is sufficient to calculate the properties of quantum structures with reasonable accuracy. To achieve proper results for higher temperatures or if quantum levels are close to the Fermi energy (in terms of kT), a *self-consistent* solution of the Poisson and Schrödinger equations is required, because of the considerable contribution of confined charge carriers to the total charge density ρ. This contribution differs from the one obtained in the classical description.

In our quantum wire the wave function $\Psi(x,y,z)$ of a single charge carrier can be separated as $\phi(y)\psi(x,z)$, where $\phi(y)$ is the unconfined part for the motion along the wire and is described by plane waves. The factor $\psi(x,z)$ is the two-dimensionally confined part. Considering a structure with quantum confinement for electrons (the consideration applies to holes analogously), $\psi(x,z)$ is determined within the one-band approximation by the effective-mass equation in the BenDaniel-Duke forms[38]

$$\mathcal{H}\psi(x,z)=E\psi(x,z), \tag{2}$$

$$\mathcal{H}=-\frac{\hbar^2}{2}\nabla\left(\frac{1}{m^*(x,z)}\nabla\right)+E_C(x,z). \tag{3}$$

$m^*(x,z)$ is the spatial-dependent (isotropic) effective mass and $E_C(x,z)$ is the conduction-band edge which acts as confinement potential. The probability density $|\psi|^2$ is used to derive a quantized electron density which is given by

$$n_q(x,z)=\sum_i N_i|\psi_i(x,z)|^2, \tag{4}$$

with i numbering all bound states. N_i is the number of electrons per unit length in the ith subband, and is given by

$$N_i=\frac{2m^*kT}{\pi^2\hbar^2}F_{-1/2}\left(\frac{E_F-E_i}{kT}\right).$$

E_F is the Fermi energy, E_i is the energy of the ith state, and $F_{-1/2}$ the Fermi integral of order $-\frac{1}{2}$.

This carrier density is used to derive a different charge density which in turn is used in the Poisson equation. Thus the Schrödinger and Poisson equations are coupled via the eigenstates (E_i,ψ_i) and the confinement potential. It has been proved that this system of equations offers a unique solution for attractive potentials.[39] The repeated successive solution of Poisson and Schrödinger equation is similar to a fixed-point iteration, and converges under certain conditions. However, the true self-consistent solution of Poisson and Schrödinger equation is seldom performed since it requires a large computational effort.

III. NUMERICAL METHODS

A. Poisson equation

Due to the required global charge neutrality the domain on which the Poisson equation must be solved is large. It amounts to up to $1\times1\,\mu\text{m}^2$ depending on doping and temperature. The shape of the domain is either trapezoidal or rectangular depending on the type of structure considered (see the light gray shaded areas in Fig. 1). The different length scales of potential variations near the boundaries of the domain and near the interface suggest the choice of an inhomogeneous orthogonal grid on which the Poisson equation is discretized. The central unit cell size is about 5×7 Å^2, and the total number of mesh points amounts to up to 100 000.

On the upper and lower borders Dirichlet boundary conditions are used in order to produce the bulk situation. On the left and right borders Neumann boundary conditions are employed in order to create mirror symmetry. If the grid is sufficiently large, these boundary conditions guarantee global charge neutrality. A useful criterion for the correct grid size is the normal derivative of the potential at the upper and lower domain boundaries. It must be zero, since the bands will relax to a flatband condition. If a solution does not meet this criterion, the size of the domain of solution must be increased.

For the discretization of the Poisson equation a five-point star difference scheme was used for the Laplacian and central difference quotients for the first derivatives. The resulting set of nonlinear equations is solved by a damped, inexact Newton iteration (following the ideas from Ref. 40) including a successive over-relaxed (SOR) solver[40,41] for the approximate inversion of the Jacobian.

B. Schrödinger equation

The Schrödinger equation is discretized on a square 200×200 unit cell grid with a mesh size of 5×5 Å^2. The differential expressions $(\partial/\partial\nu)(1/m^*)(\partial/\partial\nu)$ are replaced by a symmetrical second-order difference quotient,[42] thus converting the eigenvalue problem into a sparse matrix eigenproblem. This eigenproblem is solved by nested iteration with a generalized block Davidson algorithm using a tridiagonal preconditioner.[43,44]

The domain of solution of the Schrödinger equation (''Schrödinger box'') is significantly smaller than that of the Poisson equation, covering only the central region of the V groove (see the dark shaded areas in Fig. 1). The modified charge density Eq. (4) has to be calculated only inside the Schrödinger box, outside of it the classical expression can be used. On all boundaries of the Schrödinger box Neumann boundary conditions are applied. Additionally the iteration process has explicitly been restricted to vectors that also fulfill Dirichlet conditions. Thus the Schrödinger box possesses infinitely high barriers, and it is important to ensure that the box is sufficiently large to avoid any influence of these barriers. This is a difficult task because the confinement potential shape of a type-II interface quantum well is approximately triangular near the interface, and shows a smooth transition to a flatband towards the bulk material. The energy spectrum of bound states in such a quantum well is somewhat similar to the spectrum of hydrogen and the number of ''bound'' states is very large, but the distance between the two states decreases rapidly as their energy increases. We choose a small Schrödinger box containing, e.g., the lowest six wire states; higher states are not taken into account for the quantized charge density. Instead an instantaneous transition to the continuum above the nominally highest wire level is assumed and the contribution of higher bound states is taken into account by means of a classical charge density.

C. Self-consistency cycle

We have adopted the *extrapolated convergence factor method* originally introduced by Stern[45] for quantum wells. This is a quite simple method with practically no overhead. We have found that this method significantly improves the convergence rate and leads to greater numerical stability. The self-consistency cycle is repeated until $e\Phi$ varies by less than 10^{-3} meV. The accuracy of the result is influenced by several sources of errors. We estimate the total error to be about ±0.5 meV.

All calculations were carried out on the Cray J932/16-8192 vector computer at the Zuse-Institut-Berlin. For an average calculation of six eigenstates the desired accuracy is achieved within ten cycles and about 50-min total CPU time. About 90% of the time is consumed by the Schrödinger solver and 10% by the Poisson solver.

IV. RESULTS

In this section the results for several model systems are presented, starting with a lattice-matched $\text{InP/In}_{0.48}\text{Al}_{0.52}\text{As}$ heterojunction in a single V groove. By means of this system self-consistent and semiclassical calculations are compared, and the influence of doping and of the ''sharpness'' of the groove tip on the formation of a quantum wire is examined. In Sec. IV B the results for structures of the same material system, but with periodically arranged V grooves, are presented. Section IV C deals with the results for the type-I system $\text{GaAs/Al}_x\text{Ga}_{1-x}\text{As}$. For the sake of device relevance all calculations refer to $T=300$ K. If not stated otherwise the sidewalls of the grooves are $\{111\}$ facets forming an angle of $\alpha=70.6°$.

A. $\text{InP/In}_{0.48}\text{Al}_{0.52}\text{As}$ heterojunction in a single V groove

An $\text{InP/In}_{0.48}\text{Al}_{0.52}\text{As}$ heterojunction has been chosen because it can be grown easily by metal-organic chemical-vapor deposition (MOCVD) on planar[11] and corrugated[36] substrates. On a planar substrate and under appropriate doping conditions a type-II interface quantum well is formed, electrons are located in the InP, and holes in the $\text{In}_x\text{Al}_{1-x}\text{As}$. The MOCVD-grown $\text{In}_{0.48}\text{Al}_{0.52}\text{As}$ was always found[11] to be n doped with $N_D\geqslant10^{16}$ cm^{-3}. The nominally undoped InP had shown a slight n background. Hence we assume an n-background doping of $N_D=4\times10^{15}$ cm^{-3} for the InP. The growth sequence for the model groove is InP on $\text{In}_{0.48}\text{Al}_{0.52}\text{As}$.

We examine a groove with $\rho=10$ nm and an $\text{In}_{0.48}\text{Al}_{0.52}\text{As}$ doping level of $N_D=4.6\times10^{17}$ cm^{-3}. Figure 2 shows the calculated conduction-band profile. An attractive potential for electrons is formed in the center of the groove where two effects can be observed: First, the conduction-

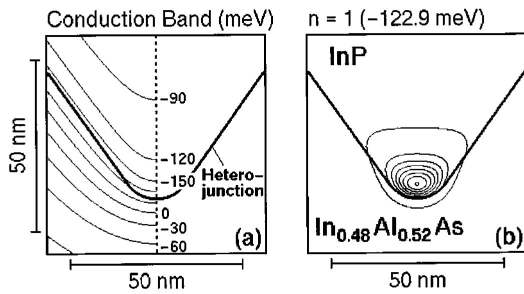

FIG. 2. Self-consistent conduction-band edge with respect to the (a) InP bulk conduction-band edge and (b) probability density $|\psi^*\psi|$ of the electron wire ground state. For better visibility, only the left half of the isolines is shown in (a); the spacing between isolines is 30 meV. The Fermi energy is below the InP bulk conduction-band edge at -127.7 meV. In (b) the outermost isoline indicates 99% probability.

band edge near the interface is shifted to lower energies in the vicinity of the groove tip. Second, the triangular-shaped type-II confinement potential at the interface becomes narrower near the tip (see Fig. 3).

The first effect is a consequence of the global charge neutrality. It requires equal space charge zones on both sides of the heterojunction. In order to maintain this balance in the vicinity of the groove tip, the InP space-charge zone is extended further away from the interface and the $In_xAl_{1-x}As$ space-charge zone is constricted around the tip. This leads to a change of the electrostatic potential shape, so that its equipotential lines do not follow the sharp bend of the interface. Hence the energy of electrons is lowered near the groove tip. The spatial extent of the space-charge zone deformation is of the order of the Debye length, which is about 65 nm for bulk InP but is expected to be less in the space-charge zone, due to the higher charge-carrier density. We estimate the average Debye length near the interface to be 20–30 nm.

The second effect can be observed only by means of self-consistent calculations. It is due to the confinement of electrons leading to a wider charge distribution, which in turn changes the electrostatic potential shape in a way that the type-II confinement potential perpendicular to the interface is narrowed. This narrowing increases the energy of confined electrons.

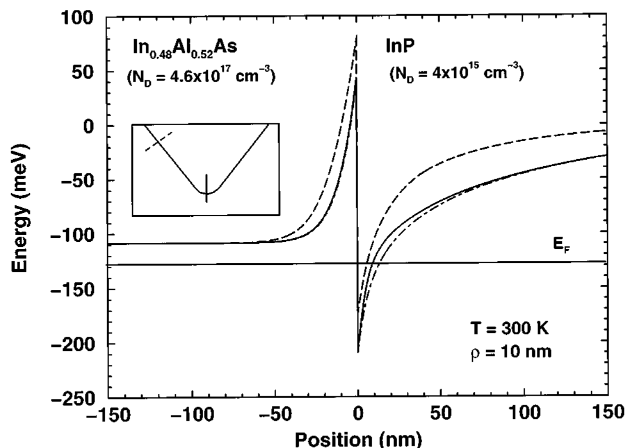

FIG. 3. One-dimensional cuts of the conduction-band edge from Fig. 2(a) perpendicular to the interface (see the inset). The dashed cut is 0.5 μm off the groove center and gives the potential shape at the flat interface. The dash-dotted line is a cut of the semiclassically calculated conduction-band profile in the center of the groove. The horizontal solid line indicates the position of the Fermi energy.

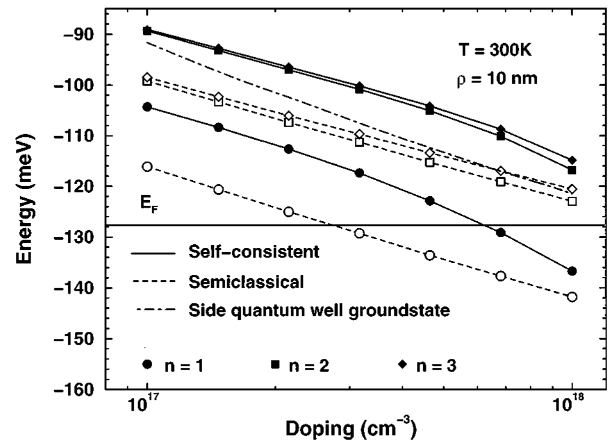

FIG. 4. Energies of the lowest three electron states in a single V-groove wire for different doping levels of the $In_{0.48}Al_{0.52}As$ layer calculated self-consistently and semiclassically, respectively. All two-dimensional states with an energy above the side quantum-well ground state are not truly bound.

Although both effects have opposite influences on the electron energies, the first one is dominant, and produces an additional potential variation parallel to the interface. In the following ''parallel'' means ''parallel to the interface.'' The parallel variation is rather shallow (see Fig. 7) compared to the perpendicular one, but it is strong enough to create a confinement in a second direction. Thus in the groove an electronic quantum wire is formed which is connected to the triangular type-II interface quantum well on the sidewalls (side quantum wells).

Due to the shallowness of the lateral potential the wire has very few bound states. In this particular example only the ground state at -122.9 meV is bound. The distance between the wire ground state and the side quantum-well ground state amounts to 10.6 meV, and is smaller than kT at room temperature, so that evaporation of electrons from the wire into the well surely will occur.

All energies of electron levels in the $InP/In_{0.48}Al_{0.52}As$ system refer to the conduction-band edge of bulk InP, which is at 0 meV. In a type-II triangular potential the usual method of measuring energies with respect to the bottom of the potential well becomes risky because the bottom is not flat. The difficulties even increase for a wire, since the minimum of the confinement potential is a single point and its energy cannot be determined exactly due to the discretization error. The problem can be solved by using the bulk InP conduction-band edge as a reference level, because it forms the upper edge of the potential well and its energy can be calculated precisely. Thus all electron energies are negative and 0 meV is the ''ionization energy.'' However, this reference level seems to be more appropriate.

The formation of a two-dimensional electron confinement potential in the center of the groove implies that the potential shape of the upper valence-band edge becomes repulsive at this place. If the layer sequence is reversed, i.e.,

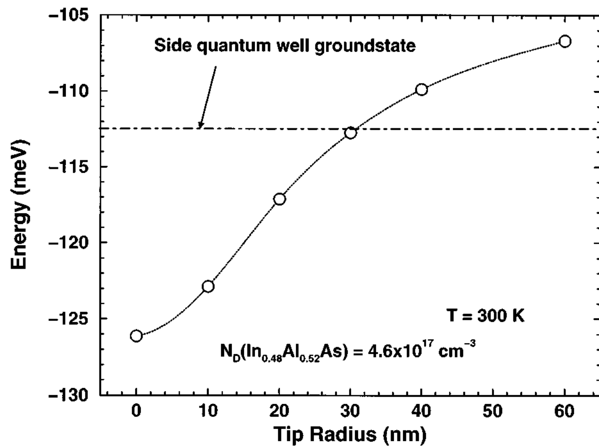

FIG. 5. Dependence of the ground-state energy on the tip radius ρ. For $\rho > 30$ nm there is no confinement. These states were calculated neglecting the side quantum well.

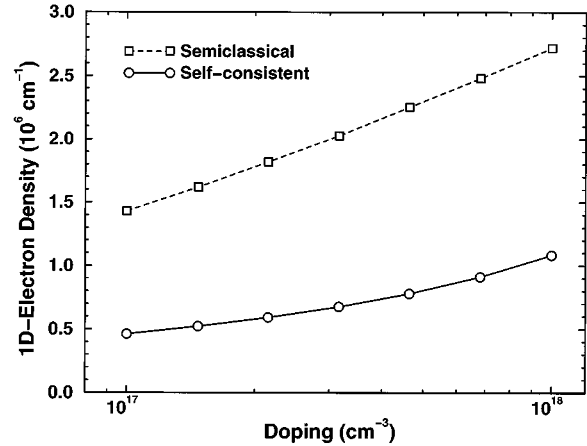

FIG. 6. Linear electron density in the quantum wire as a function of the $In_{0.48}Al_{0.52}As$ doping level. The densities are calculated according to Eq. (4) involving the *bound* states only.

$In_{0.48}Al_{0.52}As$ on InP, a hole wire in $In_{0.48}Al_{0.52}As$ is formed in the V groove. This is an important property of type-II heterojunctions, which will be discussed in more detail below.

The formation of quantum wires in a single heterojunction has several advantages: they are easy to fabricate, they suffer less from interface defects than quantum wires in double heterostructures, and there should be no spectral broadening due to size fluctuations. In the following the influence of two parameters on the band structure and the wire states will be examined: the doping of the $In_{0.48}Al_{0.52}As$ layer and the radius ρ of the groove tip.

1. Influence of doping

To demonstrate the influence of doping of the $In_xAl_{1-x}As$ layer we calculated the bound wire states for doping levels N_D between 10^{17} and 10^{18} cm^{-3} for a tip radius $\rho = 10$ nm. The energies of the wire ground state and excited states are displayed in Fig. 4 together with that of the side quantum-well ground state. The latter has been obtained from a one-dimensional self-consistent calculation. The wire states shift to lower energies with increasing doping level. This is an interesting observation, because the wire itself is located in the undoped InP. The wire states can be tuned within a certain range by doping the substrate, without introducing impurities into the quantum wire, which would reduce the electron mobility. The overall behavior is similar to that of the samples presented in Ref. 46.

The energy of the wire ground state is close to or even below the Fermi energy which is below the InP bulk conduction-band edge at -127.7 meV. Thus the thermal population of the one-dimensional subband of the ground state is high, and the formation of a one-dimensional electron gas is to be expected. This is an important feature for the design of conducting channels.

The first excited state cannot really be considered a wire state, since its energy is above the side quantum-well ground state. The transition between wire and well states cannot be properly modeled in two-dimensional calculations so that the excited states in Fig. 4 still are pure wire states that do not ''see'' the side quantum well. To some small extent they are influenced by the Schrödinger box.

2. Influence of the tip radius

In a second set of calculations the radius of the groove tip has been varied between 0 and 60 nm for a fixed $In_{0.48}Al_{0.52}As$ doping of $N_D = 4.6 \times 10^{17}$ cm^{-3}. The groove tip radius has a strong influence on the formation of the two-dimensional confinement. Figure 5 displays the energy of the wire ground state as a function of the tip radius. Additionally, the energy of the side quantum-well ground state is marked. The wire ground-state energy increases with ρ; at $\rho \approx 30$ nm it equals that of the well ground state while the wire confinement disappears. The energies for $\rho > 30$ nm are computed neglecting this effect. The increase of the ground-state energy is due to a reduction of the parallel confinement, its minimum in particular increasing as the tip radius increases. We note that the Debye length in the InP layer near the interface is 20–30 nm. Thus, if the tip radius approaches this value, the parallel confinement disappears. For device applications a small tip radius $\rho \leq 10$ nm is a prerequisite.

3. Comparison between self-consistent and semiclassical calculation

Figure 4 shows the energies of the three lowest wire states as a function of the $In_{0.48}Al_{0.52}As$ doping. In addition to the self-consistent results those obtained by the semiclassical approach are displayed. In the semiclassical calculation, yielding energies lower by about 10 meV, the first and second excited wire states are now below the side quantum-well ground state. This effect is caused by the difference between the charge densities on which the calculation of the electrostatic potential is based. As mentioned above, the inclusion of quantum effects leads to a wider and ''smoother'' charge distribution, which in turn yields a narrower perpendicular type-II potential. Hence the energies of the wire states increase (figuratively speaking the wire states are ''squeezed'' to higher energies). The difference of the potential shapes is displayed in the cuts in Fig. 3. Comparing the semiclassical and self-consistent potentials, the narrower shape of the latter becomes obvious. The difference between the energy levels

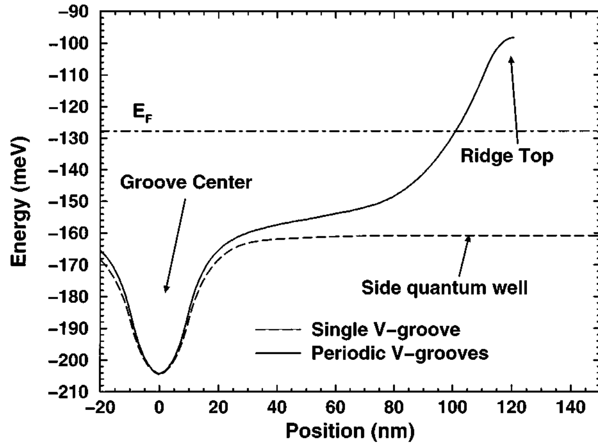

FIG. 7. Conduction-band edge along the interface. The dashed line refers to a single V groove and the solid line to a periodic groove ensemble with $\lambda = 150$ nm. The improvement of the parallel potential in the latter is evident.

is mainly due to the different perpendicular confinement potentials. In fact the parallel potential shapes are nearly identical.

The energies of the wire states determine the thermal occupation of their subbands, and incorrect energy levels will lead to wrong predictions about the electron density in the wire. To illustrate this, we have calculated the linear electron density of the wire for different doping levels of the $In_{0.48}Al_{0.52}As$, based on self-consistent and semiclassical results, respectively. In Eq. (4) we summed over all *bound* wire states, i.e., the three lowest semiclassical states and the self-consistent ground state. The result is shown in Fig. 6. The semiclassical calculation yields densities about three times larger than the more accurate self-consistent calculation.

B. $InP/In_{0.48}Al_{0.52}As$ periodical V grooves

All calculations presented so far were performed for a single V groove. Obviously the most severe problem of this structure is its small parallel confinement. One method to increase the parallel confinement is lateral p-n doping.[35] Another way to overcome this difficulty is to remove the side quantum well. This can be done by creating a periodic sequence of V grooves with small lateral distance, separated by triangular ridges [see Fig. 1(b)]. Such a ridge can be considered as a V groove with an inverse layer sequence, turned upside down. Hence the electrostatic potential near the ridge top is similar to that around a groove tip but, due to the reversed layer sequence, the parallel potential is repulsive for electrons and attractive for holes. If the distance λ between the grooves is reduced below 500 nm, which is technologically no problem, their parallel potentials will overlap. As a result the side quantum wells disappear, and evaporation into the wells is no longer possible. As a consequence, the electron wires have more bound states. Figure 7 shows the variation of the conduction band edge as a function of the position along the junction for a single V groove and a periodic structure. We have assumed identical radii ρ for ridge tops and groove tips.

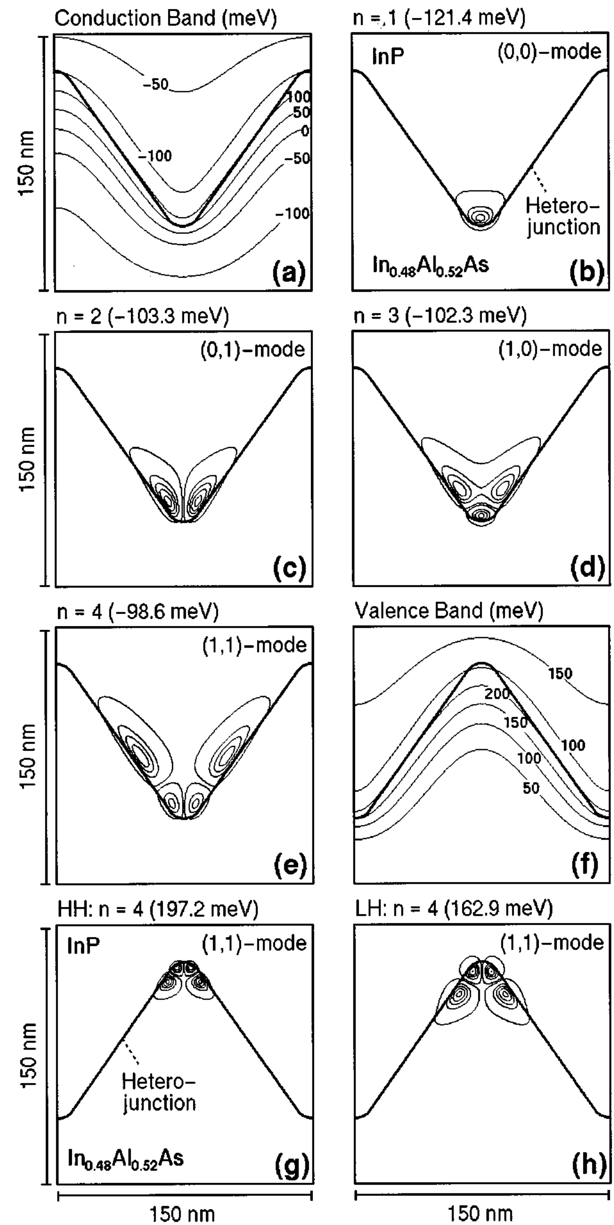

FIG. 8. (a) Conduction- and (f) valence-band edges and (b)–(e) probability densities $|\psi^* \psi|$ of selected electron and (h) hole (g) and states in a periodic groove structure with $\rho = 10$ nm, $\alpha = 70.6°$, and $\lambda = 150$ nm. All electron related energies refer to the InP bulk conduction-band edge and all hole related energies refer to the $In_{0.48}Al_{0.52}As$ bulk valence-band edge. In the band-edge plots (a) and (f), the isoline spacing is 50 meV. The Fermi energy is below the InP bulk conduction-band edge at -127.7 and 1430.8 meV above the $In_{0.48}Al_{0.52}As$ bulk valence-band edge, respectively. In pictures (b)–(e), (g), and (h), the outermost isoline indicates 99% probability.

In the type-II system $InP/In_{0.48}Al_{0.52}As$, the ridges contain quantum wires for holes, thus in a periodic structure spatially separated quantum wires for electrons and holes are formed in alternating sequence. Figure 8 shows the conduction- and valence-band profiles for such a structure with $\rho = 10$ nm, $\lambda = 150$ nm, and $N_D = 4.6 \times 10^{17}$ cm^{-3} together with isoline plots of electron and hole wave functions. The valence-band edge in the ridge forms an attractive potential for holes lying

TABLE I. The 14 lowest electron states in a periodic groove structure, $\rho=10$ nm, $\alpha=70.6°$, $\lambda=150$ nm, and $N_D(In_{0.48}Al_{0.52}As)=4.6\times10^{17}$ cm^{-3}. The wire states are arranged in pairs by the sum of quantum numbers. This systematic ordering is broken by the (0,2) mode at $n=14$. All states above $n=9$ are likely to couple to the adjacent groove. All energies refer to the InP bulk conduction-band edge.

Number	Energy (meV)	Mode	Number	Energy (meV)	Mode
1	−121.1	(0,0)	8	−92.0	(3,1)
2	−103.2	(0,1)	9	−91.0	(4,0)
3	−102.3	(1,0)	10	−87.6	(4,1)
4	−98.6	(1,1)	11	−86.4	(5,0)
5	−98.0	(2,0)	12	−82.9	(5,1)
6	−95.6	(2,1)	13	−81.5	(6,0)
7	−94.9	(3,0)	14	−80.0	(0,2)

about 1300 meV below the Fermi energy; therefore the thermal occupation of the bound states is negligible, and a self-consistent calculation of the hole states is not necessary. The energies of hole states refer to the $In_{0.48}Al_{0.52}As$ bulk valence-band edge, and are thus positive. However, in this case the reference level is not the upper barrier of the confinement potential. In the model system described here excited holes can overcome the potential barrier between $In_{0.48}Al_{0.52}As$ and InP, and do not evaporate into the bulk. Since in this process tunneling effects should be taken into account the upper edge of the wire confinement potential is not exactly defined. For this reason we think that the energy of the bulk valence-band edge constitutes a more accurate reference. Nevertheless one should keep in mind that the upper barrier of the confinement potential is at about 110–120 meV.

The electron wave functions have a symmetrical structure, and their nodelines can be identified as either vertical or horizontal. Vertical means parallel to the axis of symmetry and horizontal means perpendicular to the axis of symmetry at least at the point of their intersection. Accordingly the wire states can be labelled by two quantum numbers indicating the numbers of horizontal and vertical nodes, respectively. The ground state is the (0,0) mode, the first excited state a (0,1) mode, the second excited state a (1,0) mode, and so on. Table I gives the energies of the 14 lowest states in the electron wire. The wire states form a sequence of alternating parities up to the 14th state which is the (2,0) mode. States with the same sum of quantum numbers arrange in pairs which have a small energy splitting, indicating near degeneracy. Concerning the wave functions above the ninth state it can be safely assumed that the wave functions of adjacent grooves are coupled to form a ''wire superlattice.'' Our calculation is not well suited to describe this coupling accurately, since superlattice states cannot be normalized in two dimensions due to their Dirac vector property. The wave functions also indicate the disparity of perpendicular and parallel confinement. The first being much stronger, no states with a parallel node, corresponding to the first excited state of the type-II quantum well, can be found. The same holds true for the hole states, although the wave functions have a smaller spatial extent due to the larger effective mass and the steeper and more constricted shape of their confinement potential.

An important question is whether recombination of excess carriers generated by external excitation in the electron and hole wires is likely. In the framework of Fermi's golden rule and envelope-function theory, the transition probability is proportional to the square of the two-dimensional wave-function overlap

$$P=\int_{\mathbb{R}^2}|\psi_e\psi_h^*|d^2r \tag{5}$$

of the electron and hole wave functions ψ_e and ψ_h. We have found $P^2<10^{-8}$ for the ground state because of the large lateral distance between the electron and hole wires and the spatially indirect nature of the type-II quantum well. The wave functions overlap in a narrow zone along the interface only; its perpendicular extension is determined by the tunneling length. The perpendicular overlap zone is enlarged by the electric field in the space-charge zone (quantum-confined Stark effect) similar to the situation of a flat interface. The overlap increases further with the lateral extent of either wave function. However, even for the fourth electron and light hole states $P^2\approx6\times10^{-5}$. To give an accurate estimation of the further evolution of P by our calculations is therefore very difficult because higher states tend to couple to the adjacent grooves or ridges, respectively. In any case significant overlap is only to be expected for very high states unlikely to be populated. We have therefore come to the conclusion that effects of recombination between adjacent wires are marginal compared to type-I wires.

We have examined the influence of the tip radius ρ and the distance λ between the ridges using the same methods as for single V grooves. We have also examined the influence of doping but since the results are very similar to those of a single groove there is no need to go into a detailed discussion here. The only finding worth mentioning is that the level distance in the wires is practically not influenced by the doping level.

1. Influence of the tip radius

Figure 9 displays the energies of the five lowest wire states as a function of ρ. Similar to the single V-groove structure, the ground state shifts to higher energies with increasing ρ, while the first excited state decreases slightly. Thus the energetic separation between them is only 3.3 meV at $\rho=40$ nm. All higher states shift slightly upwards. These observations are explained by the attenuation of the parallel potential in the same way as for single V grooves.

The level crossing at $\rho\approx7.5$ nm indicates a degeneracy with vertical and horizontal nodes being equivalent. This is quite surprising, since such behavior has been observed only in highly symmetrical wire cross sections like circles or squares.

At $\rho=40$ nm the levels are nearly equidistant, but the level separation is very small. This indicates a vanishing parallel quantization by which the wire slowly transforms into a well. Only for small ρ is the distance between the ground state and the first excited state comparable to kT.

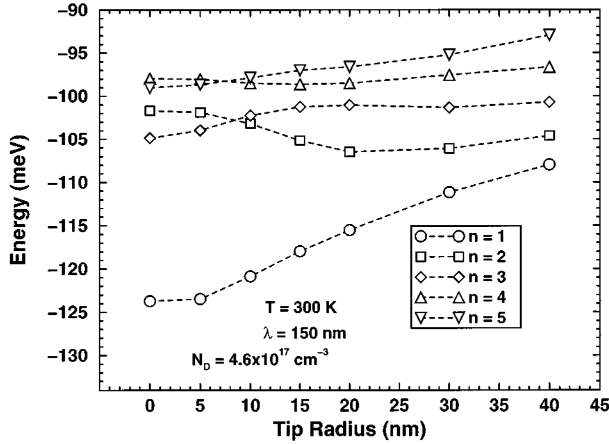

FIG. 9. Energy levels in the electron wire as a function of the tip radius ρ. An increase of the tip radius leads to a decrease of the level separation between $n=1$ and 2 which indicates an attenuation of the parallel confinement.

2. *Influence of the lateral distance*

We have varied the groove period λ between 35 and 300 nm. For $\lambda \leqslant 150$ nm the entire spectrum of the wires shifts to higher energies as λ decreases (see Fig. 10). The energy splitting between symmetrical pairs of sublevels increases, too. This fact can be explained by the influence of the lateral potential modulation. The basic idea of periodic grooves is to remove the side quantum well. However, for small λ the lateral potential modulation induced by the ridges leads to enhanced lateral confinement; in particular, excited states are influenced by this effect because of their greater spatial extension. A small groove period λ could so improve the localization in the quantum wires. Regrettably, V groove structures with λ smaller than 50 nm or below are still difficult to fabricate, and methods like electron beam lithography have to be employed. In addition the coupling between neighboring grooves is enhanced by the decreasing parallel potential barrier. That way a quantum-wire superlattice is formed which may exhibit interesting properties due to a possible lateral transport between one-dimensional states.

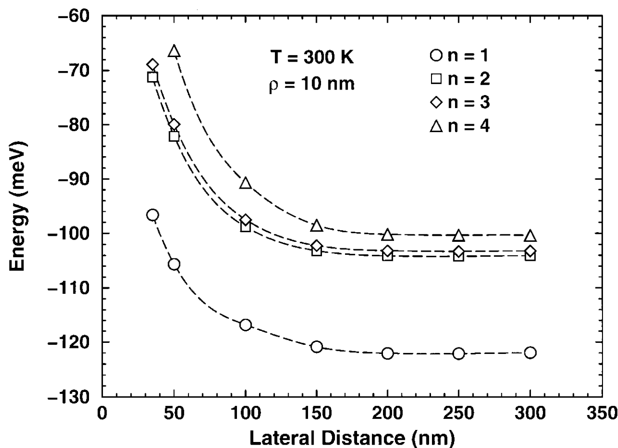

FIG. 10. Dependence of the electron levels on the lateral groove distance λ, calculated for $\rho = 10$ nm and an $In_{0.48}Al_{0.52}As$ doping of $N_D = 4.6\times 10^{17}$ cm^{-3}.

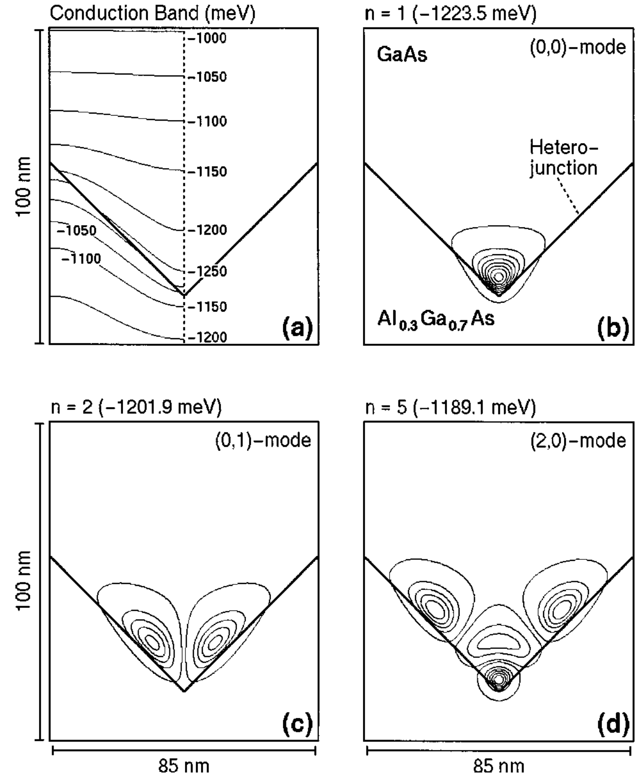

FIG. 11. (a) Self-consistent conduction-band edge and (b)–(d) probability densities $|\psi^* \psi|$ of selected electron states in a $GaAs/Al_{0.3}Ga_{0.7}As$ modulation-doped heterojunction, with $\alpha = 90°$, $\rho = 0$ nm, $\lambda = 85$ nm, $N_D(Al_{0.3}Ga_{0.7}As) = 1\times 10^{18}$ cm^{-3}, and $N_A(GaAs) = 1\times 10^{14}$ cm^{-3} (according to Ref. 34). All energies are related to the GaAs bulk conduction-band edge; the Fermi energy is at -1228 meV.

C. $GaAs/Al_xGa_{1-x}As$ type-I heterojunction

The influence of the substrate corrugation on interface quantum wells was first studied on $GaAs/Al_xGa_{1-x}As$ type-I inversion layers.[33,35] However, up to now no self-consistent calculations have been presented for this material system. Recently Vacek, Sawada, and Usagawa[34] described a corrugated, modulation-doped $GaAs/Al_{0.3}Ga_{0.7}As$ heterojunction, which forms a periodic V-groove structure with $\alpha = 90°$, $\rho = 0$ nm, and $\lambda = 85$ nm. Unfortunately neither the calculation method nor the assumed temperature were mentioned. Using a semiclassical calculation for room temperature, we arrive at results similar to the ones of Ref. 34, at least for the ground state; the shape of the conduction-band edge, however, turn out to be slightly different [see Fig. 11(a)]. This difference can be due either to different boundary conditions or temperatures, or to the Boltzmann approximation used in Ref. 34. In contrast to Ref. 34 we use the bulk GaAs conduction-band edge as a reference level for the energies of the wire states, and not the Fermi energy, which in this sample is 1228 meV below the conduction band edge. By employing self-consistent calculation we obtain a shift of 17.1 meV to higher energies, similar to the $InP/In_{0.48}Al_{0.52}As$ system. The self-consistent potential causes a moderate change in the wave functions [see Figs. 11(b)–11(d)]. The interpretation given in Ref. 34 that the quantum wire can be considered a bent quantum well with a slight lateral confinement (adiabatic approximation[24]) is no longer

valid when looking at the fact that the wire possesses bound states which are inconsistent with this explanation [see, e.g., Fig. 11(d)].

V. CONCLUSION

We have calculated the spatial dependence of the conduction- and valence-band edges of type-II heterojunctions in *V* grooves self-consistently. We have found that an attractive potential for charge carrier is formed in the groove center. This potential forms a quantum wire which is attractive for one type of charge carriers while repelling the other. We have studied the influence of structural parameters on the formation of the wire and its energy states. As a model system we used InP on $In_{0.48}Al_{0.52}As$, in which an electron wire is formed. In single *V* grooves only the ground state can be considered truly bound, while excited states evaporate into the side quantum well. The strength of the parallel confinement is heavily influenced by the sharpness of the *V* groove. The energy of the wire state can be tuned by doping the $In_{0.48}Al_{0.52}As$ layer, without introducing scattering centers into the actual wire region. The problem of evaporation can be overcome by constructing periodic structures in which triangular ridges separate the grooves in such a way that the distance between two grooves is less than 500 nm. We investigated such structures, and found that the energetic distance between levels in the quantum wires is small compared to kT, and also strongly dependent on the sharpness of the groove tip. For device applications the tip radius ρ must be significantly smaller than the Debye length. We have compared results of the self-consistent and semiclassical methods, and found that the latter yields quantization energies that are too small, leading to overestimated charge-carrier densities. The semiclassical method should not be used for quantitative calculations of strongly populated subbands.

ACKNOWLEDGMENTS

We would like to thank F. Stern (IBM Thomas J. Watson Research Center) for an informative discussion. This work was supported by Deutsche Forschungsgemeinschaft (DFG) within ‘‘Sonderforschungsbereich 296.’’

[1] L. L. Chang, L. Esaki, W. E. Howard, and R. Ludeke, J. Vac. Sci. Technol. **10**, 11 (1973).
[2] R. Dingle, A. C. Gossard, and W. Wiegmann, Phys. Rev. Lett. **34**, 1327 (1975).
[3] E. Kapon, Semicond. Semimetals **40**, 259 (1994).
[4] M. Kohl, D. Heitmann, P. Grambow, and K. Ploog, Phys. Rev. Lett. **63**, 2124 (1989).
[5] S. Koshiba, H. Noge, H. Akiyama, T. Inoshita, Y. Nakamura, A. Shimizu, Y. Nagamune, M. Tsuchiya, H. Kano, H. Sakaki, and K. Wada, Appl. Phys. Lett. **64**, 363 (1994).
[6] P. D. Wang and C. M. Sotomayor Torres, Appl. Phys. Lett. **61**, 946 (1992).
[7] D. Leonard, M. Krishnamurty, C. M. Reaves, S. P. DenBaars, and P. M. Petroff, Appl. Phys. Lett **63**, 3203 (1993).
[8] N. N. Ledentsov, M. Grundmann, N. Kirstaedter, J. Christen, R. Heitz, J. Böhrer, F. Heinrichsdorff, D. Bimberg, S. Ruvimov, P. Werner, U. Richter, U. Gösele, J. Heydenreich, V. M. Ustinov, A. Yu. Egorov, M. V. Maximov, P. S. Kop’ev, and Z. H. Alferov, in *Proceedings of the 22nd International Conference on the Physics of Semiconductors*, edited by D. J. Lockwood (World Scientific, Singapore, 1995), Vol. 3, p. 1855.
[9] Y. Arakawa and H. Sakaki, Appl. Phys. Lett. **40**, 939 (1982).
[10] B. A. Wilson, IEEE J. Quantum Electron. **24**, 1763 (1988).
[11] D. Bimberg, J. Böhrer, and A. Krost, J. Vac. Sci. Technol. A **12**, 1039 (1994).
[12] J. Böhrer, A. Krost, and D. Bimberg, J. Vac. Sci. Technol. A **11**, 1642 (1993).
[13] F. Hatami, N. N. Ledentsov, M. Grundmann, J. Böhrer, F. Heinrichsdorff, M. Beer, D. Bimberg, S. S. Ruvimov, P. Werner, U. Gösele, J. Heydenreich, U. Richter, S. V. Ivanov, B. Y. Meltser, P. S. Kop’ev, and Z. H. Alferov, Appl. Phys. Lett. **67**, 656 (1995).
[14] C.-K. Sun, G. Wang, J. E. Bowers, B. Brar, H.-R. Blank, H. Kroemer, and M. H. Pilkuhn, Appl. Phys. Lett. **68**, 1543 (1996).
[15] E. R. Glaser, B. R. Bennett, B. V. Shanabrook, and R. Magno, Appl. Phys. Lett. **68**, 3614 (1996).
[16] R. Zimmermann and D. Bimberg, J. Phys. (France) IV **3**, 261 (1993).
[17] H. Kroemer and G. Griffiths, IEEE Electron. Dev. Lett. **4**, 20 (1983).
[18] S. J. Hsieh, E. A. Patten, and C. M. Wolfe, Appl. Phys. Lett. **45**, 1125 (1984).
[19] E. J. Caine, S. Subbanna, H. Kroemer, and J. L. Merz, Appl. Phys. Lett. **45**, 1123 (1984).
[20] E. Lugagne-Delpon, P. Voisin, and M. Voos, Appl. Phys. Lett. **60**, 3087 (1992).
[21] D. S. Citrin and Y.-C. Chang, J. Appl. Phys. **68**, 161 (1990); Phys. Rev. B **40**, 5507 (1989).
[22] Y. Arakawa, T. Yamauchi, and J. N. Schulman, Phys. Rev. B **43**, 4732 (1991).
[23] G. A. Baraff and D. Gershoni, Phys. Rev. B **43**, 4011 (1991).
[24] E. Kapon, D. M. Hwang, and R. Bhat, Phys. Rev. Lett. **63**, 430 (1989).
[25] M. Grundmann, O. Stier, and D. Bimberg, Phys. Rev. B **50**, 14 187 (1994).
[26] S. E. Laux and F. Stern, Appl. Phys. Lett. **49**, 91 (1986); S. E. Laux and A. C. Warren, Proc. Int. Electron Devices Meeting **86**, 567 (1986).
[27] T. Kerkhoven, A. T. Gallick, U. Ravaioli, J. H. Arends, and Y. Saad, J. Appl. Phys. **68**, 3461 (1990).
[28] T. Kerkhoven, M. Raschke, and U. Ravaioli, Superlatt. Microstruct. **12**, 505 (1992).
[29] Z. Wu and P. P. Ruden, J. Appl. Phys. **74**, 6234 (1993).
[30] C. R. Proetto, Phys. Rev. B **45**, 11 911 (1992).
[31] J. H. Luscombe, A. M. Bouchard, and M. Luban, Phys. Rev. B **46**, 10 262 (1992).
[32] M. Tadić and Z. Ikonić, Phys. Rev. B **50**, 7680 (1994).
[33] A. Sawada, T. Usagawa, S. Ho, and K. Yamaguchi, Appl. Phys. Lett. **60**, 1492 (1992).
[34] K. Vacek, A. Sawada, and T. Usagawa, Appl. Phys. Lett. **65**, 3096 (1994).

[35] W. Porod, H. K. Harbury, and S. M. Goodnick, Appl. Phys. Lett. **61**, 1823 (1992).

[36] M. Kappelt, V. Türck, M. Grundmann, H. Cerva, and D. Bimberg, *Proceedings of the Eigth International Conference on Indium Phosphide and Related Materials, Schwäbisch Gimünd, 1996* (IEEE, New York, 1996).

[37] M. Kappelt, M. Grundmann, A. Krost, V. Türck, and D. Bimberg, Appl. Phys. Lett. **68**, 3596 (1996).

[38] D. J. BenDaniel and C. B. Duke, Phys. Rev. **152**, 683 (1966).

[39] R. Illner, P. F. Zweifel, and H. Lange, Math. Methods Appl. Sci. **17**, 349 (1994).

[40] W. H. Press, S. A. Teukolsky, W. T. Vetterling, and B. P. Flannery, *Numerical Recipes in C*, 2nd ed. (Cambridge University Press, Cambridge, 1992).

[41] O. Axelsson, *Iterative Solution Methods* (Cambridge University Press, Cambridge, 1996).

[42] T. L. Li and K. J. Kuhn, J. Comput. Phys. **110**, 292 (1994).

[43] C. W. Murray, S. C. Racine, and E. R. Davidson, J. Comput. Phys. **103**, 382 (1992).

[44] E. R. Davidson, Comput. Phys. **7**, 519 (1993).

[45] F. Stern, J. Comput. Phys. **6**, 56 (1970).

[46] V. Türck, O. Stier, F. Heinrichsdorff, M. Grundmann, and D. Bimberg, Appl. Phys. Lett. **67**, 1712 (1995).